Histomorphological investigations of the avian tarsometatarsus developed from three independent periosteal bone collars

Shinji Usami

Department of Anatomy,

Nihon University School of Dentistry

(Directors: Prof. Keitaro Isokawa and Assoc. Prof. Yosuke Yamazaki)

Table of Contents

The following two articles are part of this doctoral dissertation:

The Anatomical Record 293(9), 1527-1535, 2010, doi 10.1002/ar.21179
Journal of Oral Science, in press

Abstract

Long bone morphogenesis goes through a multistep process and generates a diverse but a defined morphology that meets its functional needs. An avian tarsometatarsal (TMT) skeleton spanning from the base of toes to the intertarsal joint is a compound bone developed by elongation and lateral fusion of three initially independent periosteal bones, which are referred to as bone collars or later on cylinders. Ontogenetic development of the TMT skeleton is likely to recapitulate the changes occurred during evolution to birds from their common ancestor with theropod dinosaurs, but so far has received less attention. Therefore, in the present study, development of the embryonic TMT skeleton in domestic fowl (*Gallus gallus*) was investigated morphologically and histologically.

Three metatarsal cartilage rods radiating distally earlier in development became aligned parallel to each other by embryonic day 8 (ED8). Calcification initiated at ED8 in the midshaft of cartilage formed bone collars, and the latter extended cylindrically along cartilage surface. Coordinated radial growth by fabricating bony struts and trabeculae resulted in the formation of three independent bone collars or cylinders, which further became closely apposed with each other by ED13 when the periosteum began to fuse in a back-to-back orientation. Bony trabeculae connecting adjacent cylinders emerged first at ED17 in the dorsal and ventral quarters of intervening tissue at the mid-diaphyseal level. The cylinders were stably fused with each other and took on the surface appearance of a single compound bone by ED20, although the marrow cavities derived from three cylinders were still separated by bony septa at the fusion plane. Osteogenic cells visualized by histochemistry for alkaline phosphatase were localized preferentially in the periosteum which covers radially growing bone cylinders, and thus cancellous spaces in the wall of bone cylinders were left open widely. Contrarily, osteoclasts possessing tartrate-resistant acid phosphatase were observed later than ED10 and localized preferentially in endosteal surfaces. In the fusion of bone cylinders, trabecular bridges were formed by periosteal osteogenic cells, and the removal of bone septum was carried out by endosteal osteoclasts.

These findings suggest that the observed bone microstructure, especially a slanted

orientation of intertrabecular channels in which blood vasculature resides, is closely related to a rapid longitudinal growth of TMT skeleton, and also that the rapid radial growth does proceed by osteoblasts which reside preferentially in periosteum and postpone the osteonal filling of intertrabecular channels during embryonic periods. The fusion process of bone cylinders appeared to be managed through periosteal osteogenic cells and endosteal osteoclasts, both of which constitute an ordinary process of the long bone development.

Chapter 1: Development of the tarsometatarsal skeleton by the lateral fusion of three cylindrical periosteal bones in the chick embryo (*Gallus gallus*)

Yuichi Namba, Yosuke Yamazaki, Maki Yuguchi, Shigeo Kameoka,
Shinji Usami, Kazuya Honda and Keitaro Isokawa
The Anatomical Record 293(9), 1527-1535, 2010

Introduction

Skeletogenesis in the developing limb bud is a series of complicated developmental events comprising pattern formation of prospective skeletal elements in the seemingly homogenous mesenchymal tissue (Saunders, 1947; Todt and Fallon, 1986; Isokawa et al., 1992), osteoblastic differentiation and subsequent controlled-ossification, and morphogenesis of individual skeletal elements (Caplan and Pechak, 1987; Hartmann and Tabin, 2000; Bandyopadhyay et al., 2008). Chick limb bud has been serving as a useful experimental model for investigating all of these aspects of skeletogenesis. Among bones in the chick appendicular skeleton, tarsometatarsal (TMT) bone is notably peculiar in its morphogenesis, because it arises from three independent metatarsal primordia (and some ankle elements) but transforms into a single compound skeleton with long bone morphologies. A proximodistal elongation and radial growth of initially independent long bones must be closely related to the process of their lateral fusion. It seems however that ontogenetic development of the chick TMT skeleton has received less attention than long bone development in the thigh and shank (Caplan and Pechak, 1987).

The TMT skeleton in birds spans from the base of toes to the intertarsal ankle joint, at which the bone articulates with a tibiotarsal bone in the shank, a lower part of leg below the knee (Lucas and Stettenheim, 1972). Legs with the elongated TMT skeleton are generally interpreted as a behavioral adaptation for locomotion or prey capture (Zeffer and Norberg, 2003). Typically, the elongated TMT skeleton in ratites increases their maximum stride length while keeping large fleshy muscles in the more proximal part of the leg. This kind of leg elongation appears to be biomechanically reasonable for fast runners not only in ratites but also in many terrestrial tetrapods. A prime evolutionary example is the changes from short fore and hind foot with multiple toes in the early ancestors of perissodactyls to a large and elongated foot with a single

toe in the modern horse, Equus (MacFadden, 1988). Compared with an overwhelming growth of the third toe in Equus, developmental processes of the avian TMT skeleton, which may also recapitulate the changes occurred in the evolutionary history (Holtz, 1995; Dingus and Rowe, 1997), are likely to be more complicated because a fusion between three metatarsal elements needs to be incorporated coordinately into the longitudinal and radial growth of individual metatarsals.

In this study focusing on embryonic development of the chick TMT skeleton, the longitudinal and radial growth as well as the process of lateral fusion were examined in details morphologically, by using i) whole mount specimens for bone and cartilage staining and micro CT analysis, ii) isolated bones for measurement and scanning electron microscopy (SEM), and iii) tissue sections for histology and immunofluorescence staining of fibrillin to delineate periosteum; fibrillin is a component of microfibrils rich in the developing periosteum (Everts et al., 1998; Yamazaki et al., 2007a). Temporospatial changes observed in bone morphology and its microstructures indicate that a rapid growth of the TMT skeleton is closely related to bone vascularization and that a lateral fusion to generate a compound TMT bone is a chronologically late event in the embryonic TMT development.

Materials and Methods

Preparation of Specimens

Fertilized eggs of White Leghorn (*Gallus gallus*) obtained from Oohata hatchery (Shizuoka, Japan) were incubated at 39ºC in a humidified incubator (MTI-201A; EYELA, Tokyo, Japan). Embryos without any gross developmental defects were staged according to the morphological criteria by Hamburger and Hamilton (1951) but denoted in embryonic days (ED) in this report, to provide the sense of absolute time in development. ED6- and ED7-leg specimens were obtained from embryos at stage 29 and 32, respectively. Specimens of ED8-20 were excised from embryos at stage 34-46; at ED8 or later, ED numeral plus 26 represents the stage-numeral, for example, ED8 is equivalent to stage 34 (8 plus 26). Hindlimbs shortly after hatching were labeled as P1.

Specimens for whole mount staining with alcian blue and alizarin red and those for immunohistochemical staining were fixed in 4% paraformaldehyde (PFA) in

phosphate-buffered saline (pH 7.35; PBS) for 2 hr at 4ºC. Specimens for histological and SEM observations were fixed in 2.5% glutaraldehyde (GA) in PBS for 2 hr at 4ºC. All the procedures were carried out in accordance with a guideline by the Animal Experimentation Committee of Nihon University School of Dentistry, which is in compliance with the Nation Act on Welfare and Management of Animals.

Whole Mount Staining of Bone and Cartilage

A protocol by Kelly and Bryden (1983) was slightly modified and used for visualizing bone and cartilage in the TMT segment of leg. Briefly, PFA-fixed, rinsed specimens were immersed overnight (for about 16 hr) in 70% ethanol and then stained overnight in 0.01% alcian blue solution: 10 mg of alcian blue 8GX (C.I. 74240; Wako Pure Chemical Industries, Osaka, Japan) in 80 mL of 95% ethanol plus 20 ml of 99.7% acetic acid. Alcian blue-stained specimens were rinsed and neutralized overnight with 1% potassium hydroxide (KOH) in 70% ethanol, rehydrated in decreasing graded ethanols, and stained for 24 hr in 0.002% (w/v) alizarin red S (C.I. 58005; Wako) in 0.5% KOH. After rinsing, specimens were macerated in 2.0% KOH at room temperature and cleared successively in 3:1, 1:1, and 1:3 mixtures of 0.5% KOH and glycerin for 8-24 hr each. Specimens stained solely with alizarin red were also processed similarly. The stained and cleared whole mount specimens were kept in glycerol/ethanol (1/1) and examined under an Olympus SZ61 stereomicroscope equipped with a digital camera (C-5050; Olympus).

Measurement and SEM Observation of Bony Skeleton

Bony skeleton in the TMT was isolated from GA-fixed hindlimb at ED8-18 and P1. Tissues other than bone were dissolved completely by soaking leg specimens in 4N KOH at 37ºC for 1-3 overnights depending on the size of specimen. Isolated TMT skeleton was rinsed thoroughly and photographed under a stereomicroscope (SZ61; Olympus) equipped with a CCD camera (DS-Fi1-L2; Nikon Inc., Tokyo, Japan) for digital recording. The length of TMT skeleton was measured on the calibrated digital images. The numbers of TMT skeleton analyzed were 21, 18, 24, 30, 24, 30, 24, 12, 18, 18, and 12 for ED8-18, respectively.

For SEM observation, specimens were dehydrated in graded ethanol and dried

with a critical point dryer (HCP-2; Hitachi). Dried specimens were coated in an osmium coater (HPC-1S; Vacuum Device, Ibaraki, Japan) for 20 sec and observed with a Hitachi S-4300 field emission SEM operated at 15 kV.

Imaging by Micro-CT

Some of GA-fixed TMT segment of hind leg without KOH maceration were analyzed by a micro X-ray CT system (R_mCT; Rigaku, Tokyo, Japan) with the exposure of 90 kV, 150 μA, and slice intervals at 20 μm. Tomograms and their 3D rendering images were examined by i-View software (J. Morita, Kyoto, Japan).

Histological Observation

Plastic-embedded sections of TMT at ED6-10, 13, 17, and P1 were prepared for histological observations. Briefly, GA-fixed specimens except for those at ED6-10 were decalcified in Morse's solution; 10% citrate and 22.5% formic acid (Morse, 1945). Decalcified and undecalcified specimens were postfixed in 1% OsO4 in 0.1 M phosphate buffer (pH 7.3) for 2 hr at room temperature, dehydrated in graded ethanol and propylene oxide, and embedded in a low-viscosity epoxy resin (Spurr, 1969). Thin sections (1 μm in thickness) were prepared transversely at mid-diaphysis, stained with 1% toluidine blue and examined with a Nikon microscope (Eclipse E600) equipped with a CCD camera (Pro600ES; Pixera, Co., Santa Clara, CA, USA).

Immunohistochemistry

Specimens of PFA-fixed TMT at ED7 and 8 were cryoprotected, embedded in OCT Compound (Tissue-Tek^{TM}; Miles, Inc., Elkhart, IN, USA) and frozen in liquid nitrogen-cooled 2-methyl butane (Isokawa et al., 1994). PFA-fixed specimens at ED10, 13, and 17 were embedded in 5% carboxymethyl cellulose (CMC), according to the procedure by Kawamoto and Shimizu (2000). Frozen sections were prepared transversely from the mid-diaphysis; a transfer film method (Kawamoto, 2003) was used to obtain undecalcified frozen sections from CMC-embedded tissue at ED10 or later.

Indirect fluorescence immunohistochemistry was performed. Briefly, sections equilibrated and blocked in 1% bovine serum albumin (BSA)-PBS for 1 hr were reacted

with mouse anti-chick fibrillin-2 IgG (undiluted hybridoma conditioned medium of FB1; Isokawa et al., 2004; Yamazaki et al., 2007b) for 1 hr and washed in PBS. Sections were subsequently incubated in fluorescein-isothiocyanate-conjugated goat anti-mouse IgG for 1 hr. After washing in PBS, sections were mounted with SlowFade^{TM} (Light Antifade Kit; Molecular Probes) and examined with a Nikon epifluorescence microscope (Eclipse E600) equipped with a CCD camera (Pro600ES; Pixera). Controls by omitting FB1 antibody or replacing FB1 with nonimmune mouse IgG gave no specific immunofluorescence.

Results

Morphogenesis and Longitudinal Growth of the TMT Skeleton

Morphogenesis and longitudinal growth of the TMT skeleton were examined in whole mount preparations stained doubly with alcian blue and alizarin red (Fig. 1) and in measurement of the length of developing bone cylinders (BCs) (Fig. 2). Three metatarsal cartilage rods, which were radiating distally in the autopodium earlier in development, became aligned parallel to each other by ED8; i.e., proximal autopodium transformed its shape from a fan-like to a columnar morphology, which resulted in the formation of a distinct TMT segment between toes and tibiotarsus (ED8 or later in Fig. 1). Alizarin red staining in the TMT segment was first observed in the mid-diaphyseal portion of cartilage rods at ED8.

As the elongation of cartilage rods proceeded, calcified bone extended cylindrically on the surface of cartilage in the proximal and distal directions (Figs. 1 and 2). Cartilage surrounded by bone was progressively eroded and replaced by bone marrow tissue (Figs. 3 and 4), but this erosion proceeded somewhat slower than the longitudinal extension of BCs. Metaphyses remained cartilaginous and a considerable amount of cartilage was retained in the inside of BCs. Cartilage surrounded by cylindrical bone was hardly stained blue because the calcified bone prevented dye penetration (compare ED10 in Fig. 1 and in Fig. 4A).

Developing periosteal bones with a cylindrical morphology became closely apposed laterally and appeared to coalesce into a TMT skeleton (Fig. 1), although actual bony fusion occurred at ED17 or later as described below. Elongation of BCs in the

lateral side deviated anteriorly or posteriorly from their original axes, whereas a centrally-located cylinder developed as a bone with a ventrally-curved proximal metaphysis and a dorsally-curved distal metaphysis (Figs. 1 and 5F), indicating that morphogenesis for a compound TMT skeleton proceeds characteristically in all three dimensions before actual fusion takes place.

Onset of Calcification in Initial Bone Collars

Cartilage observed in the cross-sections of a fan-like autopodium at ED6 was surrounded by incomplete layers of perichondral oblong cells (Fig. 3A and B). The layers developed into a distinct perichondrium by ED7, but there was no apparent histological indication of osteoid deposition yet (Fig. 3C and D). At ED8, the mid-diaphyseal portion of cartilage containing hypertrophied chondrocytes was surrounded by a thin layer of densely stained, partially calcified osteoid matrix (Figs. 1 and 3E-G). It appeared that the onset and progression of calcification were slightly variable and that the cylinders were incomplete and fragile at ED8; an intact BC, such as the one in Figure 3G was rarely isolated (less than 10%, n = 21) after alkaline corrosion of ED8-specimens. In contrast, BCs of ~1.5-2.0 mm in length were regularly isolated at ED9 (Fig. 2), and the formation of vertical mineralized struts became obvious in the mid-diaphysis (Fig. 3H and I).

Radial Growth of Bone Cylinders

Radial growth for a transition from the initial simple bone collar to the cylinders of periosteal bone took place through the formation of bony struts and trabeculae (Figs. 3H, I and 4). Bony struts emerged first in the middiaphysis, and their distribution spread to both proximal and distal directions. Subsequent bone growth was apparently associated with vascularization in the periosteal tissue. Namely, fabrication of bony trabecular struts created numerous channels containing blood vasculature (Caplan and Pechak, 1987; Yamazaki et al., 2011). Channels observed as spaces in the branching network of trabeculae were slightly slanted to the long axis of a BC (Fig. 4D and F). These channels run largely parallel to each other and were interconnected via foramina. Many lacunae of about the size of cell were found on the surface of struts and trabeculae, suggesting the abundance of osteoblasts about to be entrapped in the growing bone (Fig.

4F and G).

Three developing BCs in the TMT segment were closely apposed laterally by ED13. In transverse sections (Fig. 4D), a cylinder in the middle appeared rectangle and the other two in the side was semicircular. However, there was no bony connection or fusion between these BCs, and each remained surrounded by its own periosteal tissue (Fig. 4E). Actually, the three cylinders could be isolated separately after alkaline maceration, and the surfaces confronting each other were flat and lacked a trabecular appearance, although cell lacunae suggesting a continued deposition of bone were observed in these flat surfaces (Fig. 4G).

Lateral Fusion of BCs

Fusion between adjacent BCs took place at ED17 by sharing bony trabeculae in the intervening tissue between cylinders. Initial fusion was mediated through only a small number of trabeculae present in the dorsal and ventral quarters of intervening tissue at mid-diaphysis (Fig. 5A). Possibly because of fragility of these connecting trabeculae, TMT skeleton at ED17 was still often and easily split into each cylinder during alkaline maceration (Fig. 5B and C); one or both of the lateral cylinders was separated from the middle one in about 40% of cases (n = 18). Thereafter bone fusion proceeded, and cylinders became inseparable even after complete removal of surrounding soft tissue. At P1, diaphysis appeared as a single compound bone, whereas its proximal and distal metaphyses retained morphologies alluding to original three cylinders (Fig. 5D-G).

Fusion of BCs could be expected to accompany the formation of a common medullary cavity. In the mid-diaphysis at later than ED17, communicating channels through a bony septum between medullary cavities were found, but it was also confirmed in the histological sections and CT tomograms that the septum itself was not removed completely even at P1 (Fig. 5D and F). Septum in the metaphyses appeared more robust than that in the mid-diaphysis.

Transition of Periosteum

To examine topological changes of periosteum during bone fusion in the TMT segment, immunohistochemistry for fibrillin was conducted. Fibrillin immunoreactivity

highlighted perichondrium at ED7 and periosteum at ED8 (Fig. 6A and B). Fibrillin-positive microfibrils parallel to the long axes of BCs were accumulated significantly in an outer periosteal layer but scarce or absent in an inner osteogenic cell layer of the periosteum. It was thus possible to follow the temporal alterations of periosteum with a polarity.

At ED8, periosteum ensheathed each of the initial bone collars independently. In the intervening tissue between adjacent bones, double periosteum in a back-to-back orientation came close to each other by ED10 and fused in part by ED13 (Fig. 6C and D). Additionally, fibrillin-positive matrix (asterisks in Fig. 6C and E), which emerged by ED10 and filled the ditch between cylinders, appeared to aid in the formation of periosteum to encapsulate all of three BCs together. At ED17, periosteum between cylinders disappeared first from its periphery but remained intercalated in the middle of the intervening tissue between BCs (Fig. 6E and F).

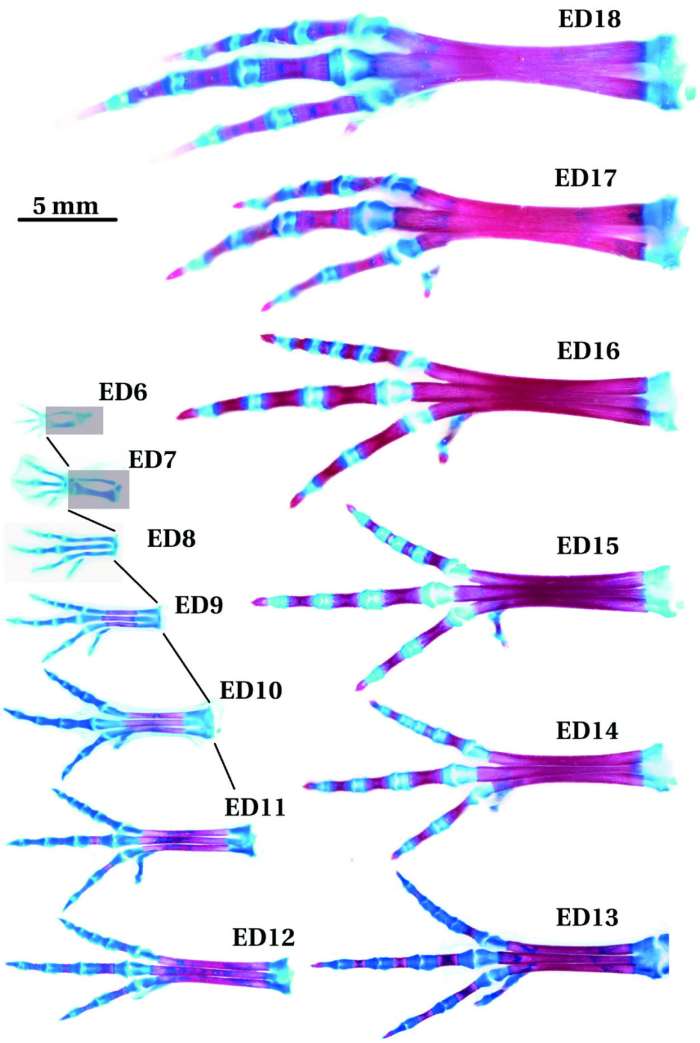

Fig. 1. Whole mount preparations of a TMT segment and toes of the developing leg buds at ED6-18. All the specimens are stained with alcian blue for cartilage and alizarin red for bone. Shaded in rectangles are primordia for tibiotarsal skeleton, or shank (ED6 and 7) and for more mesial, thigh skeleton (ED6). Bar = 5 mm.

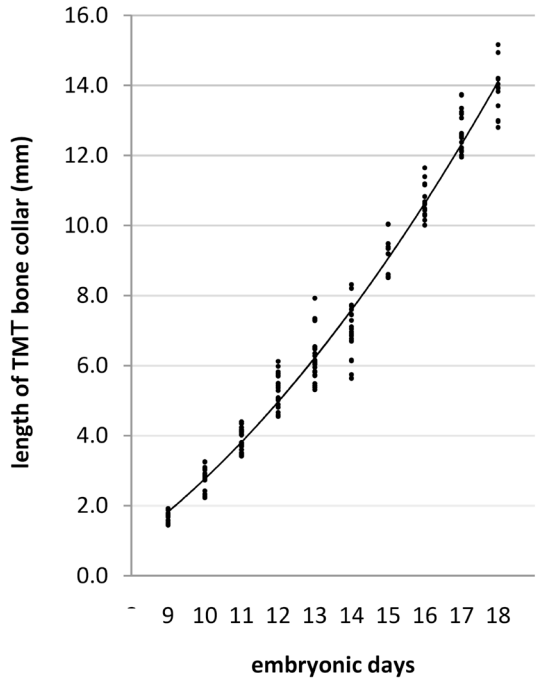

Fig. 2. Scatterplot of longitudinal growth of the TMT bone cylinders. Lengths of isolated bone cylinders at ED9-18 are plotted and a polynomial approximating curve is drawn.

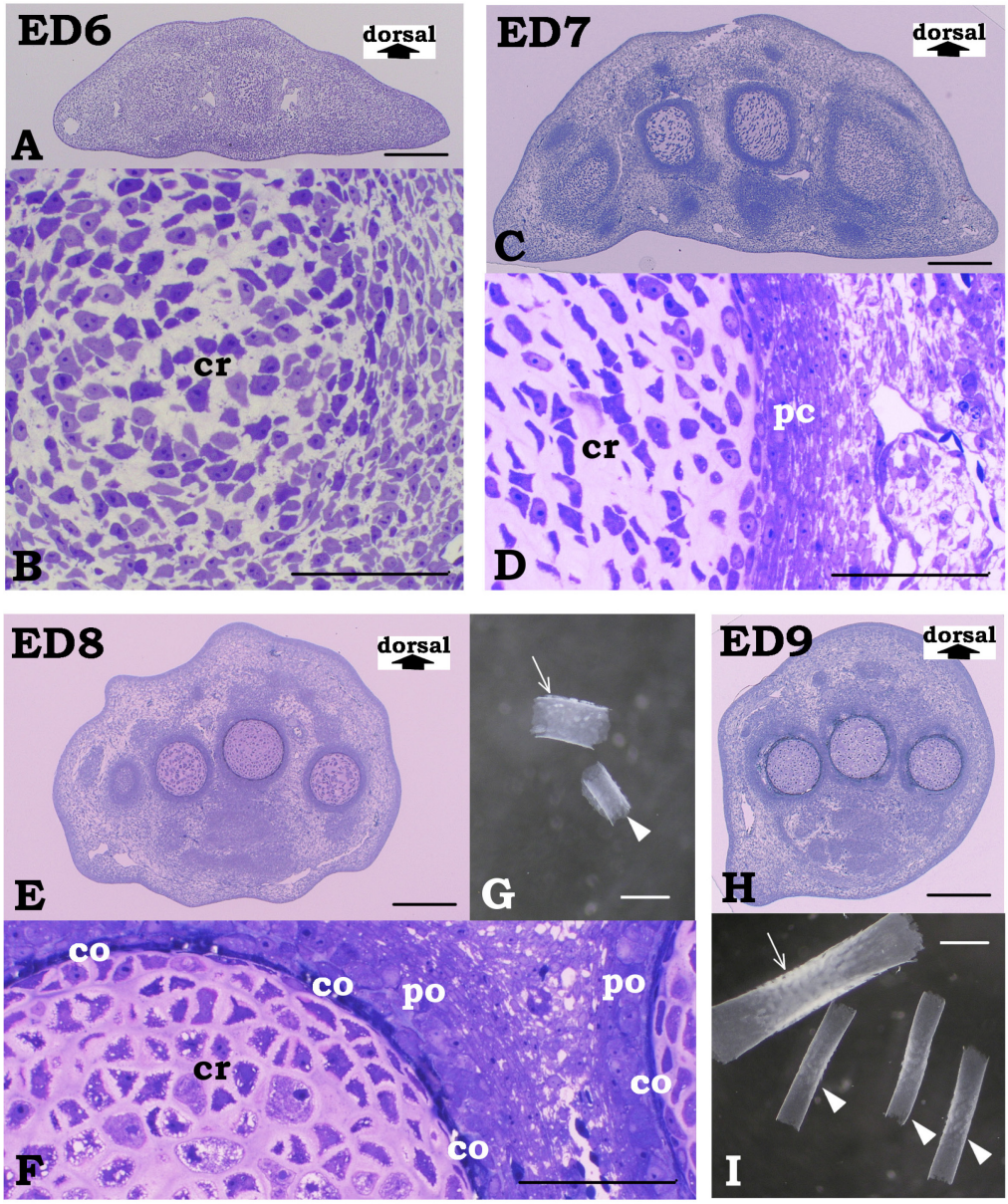

Fig. 3. Development of the TMT skeleton at ED6-9. Cross-sections at mid-diaphysis are shown at ED6 (A, B), ED7 (C, D), ED8 (E, F), and ED9 (H). Cartilage (cr) is surrounded by incomplete layers of perichondral oblong cells at ED6 and by a distinct perichondrium (pc) at ED7. Initial simple bone collar (co) surrounded by periosteum (po) is formed at ED8. Also shown are isolated bone collars (or cylinders) at ED8 (G) and ED9 (I); small slender ones (arrowheads) are isolated from the TMT segment, and large thick ones (arrows) are from tibial skeleton in the shank. Opacities discernible in the mid-diaphysis (I) represent the formation of bony vertical struts on the surface of bone collars (see also Figure 4B and C). Bars = 50 μm (G, I), 200 μm (A-F, H)

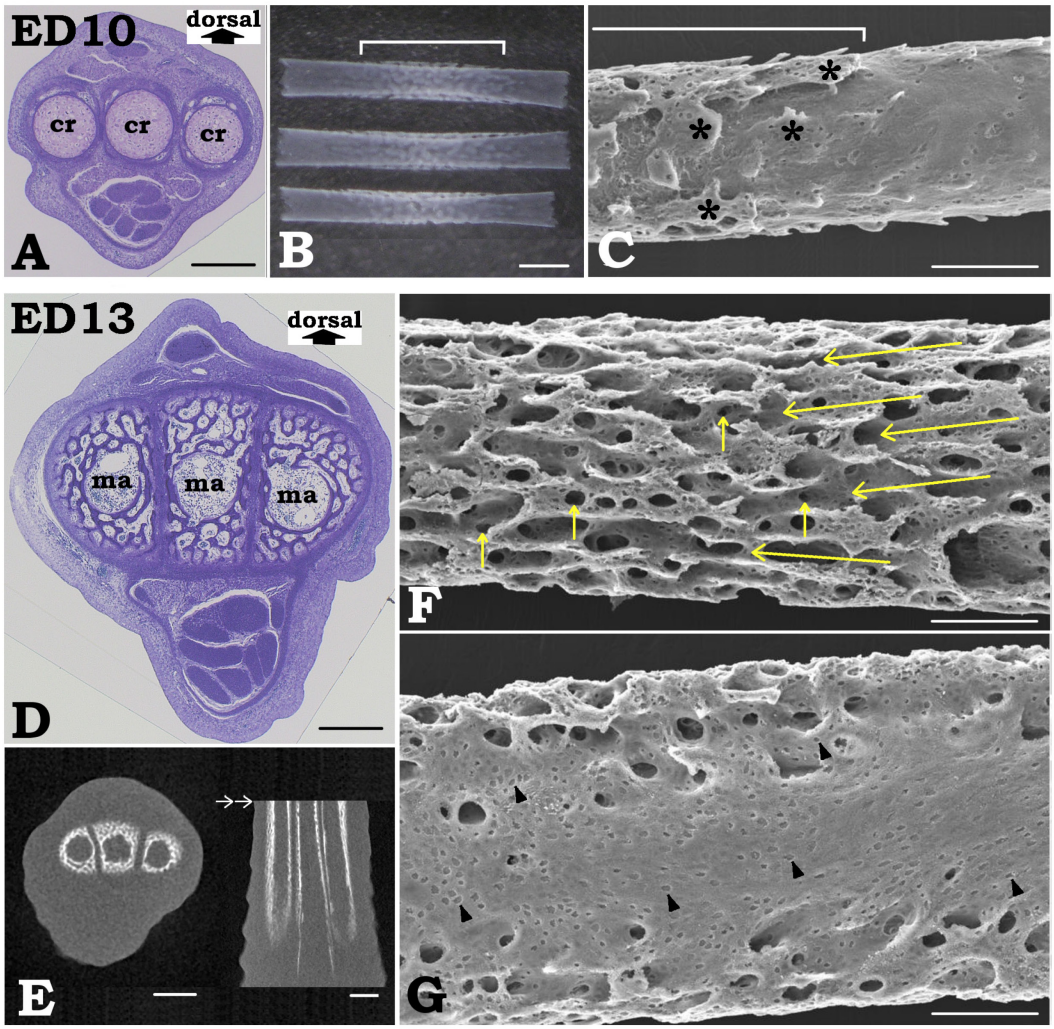

Fig. 4. Development of the TMT skeleton at ED10 (A-C) and ED13 (D-G). Histological sections at the mid-diaphysis (A, D), isolated bone cylinders (B, C, F, G) and CT tomograms (E) are shown. Mid-diaphysis (brackets in B and C) at ED10 is decorated with bony struts (asterisks). At ED13, branching network of trabeculae holding multiple channels (horizontal arrows) with transmural foramina (vertical arrows) is observed in bone cylinders (F), while the surfaces for fusion are flat and scarce in trabeculae (G). Note many lacunae (arrowheads) for osteoblasts about to be entrapped in bone. CT tomograms indicate no bony connections between adjacent bone cylinders (E); upper edge (white double arrows) of a longitudinal tomogram in the right corresponds to the plane for a mid-diaphyseal tomogram in the left. cr; cartilage, ma; bone marrow. Bars = 50 μm (B, E), 200 μm (A, C, D, F, G)

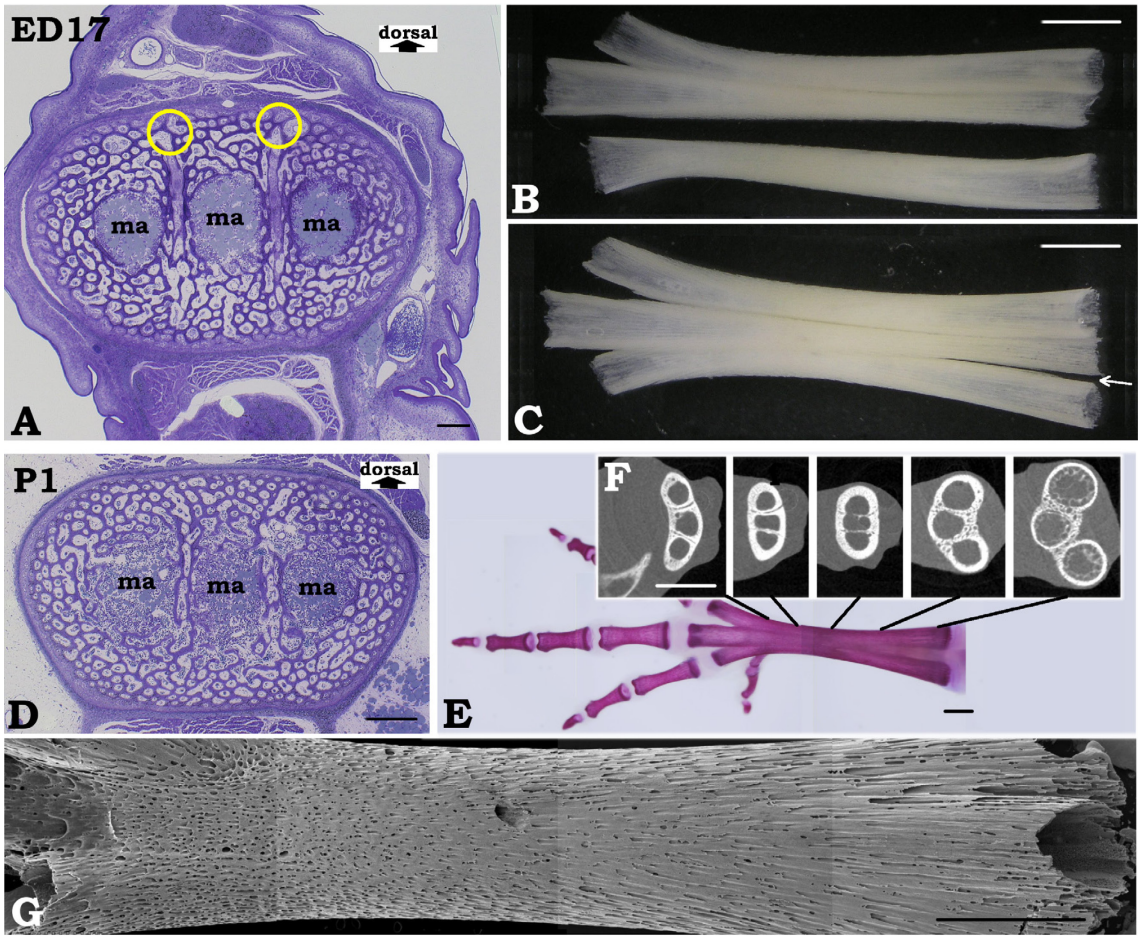

Fig. 5. Development of the TMT skeleton at ED17 (A-C) and P1 (D-G). Histological sections at the mid-diaphysis (A, D), isolated bone cylinders (B, C, G), and a whole mount specimen stained with alizarin red (E) are shown. Fusion of cylindrical bones mediated by trabeculae is observed. Connecting trabeculae (encircled in yellow) appear few in number at ED17 and bone cylinders are often separable (B). Even in the inseparable case (C), the fusion is not necessarily extensive, and a deep slit (arrow) toward mid-diaphysis can be found between cylinders. At P1, however, the TMT skeleton is a single compound bone (G; ventral aspect) without apparent ditch in the bone surface corresponding to the interface of fusion. While medullary cavities are connected through channels (D), five representative CT tomograms (F) at the different levels along the TMT skeleton (E; dorsal aspect) show that the septum itself persists. In the tomograms (F), dorsoventral axis is oriented right-to-left. ma; bone marrow. Bars = 200 μm (A, D), 2 mm (B, C, E-G)

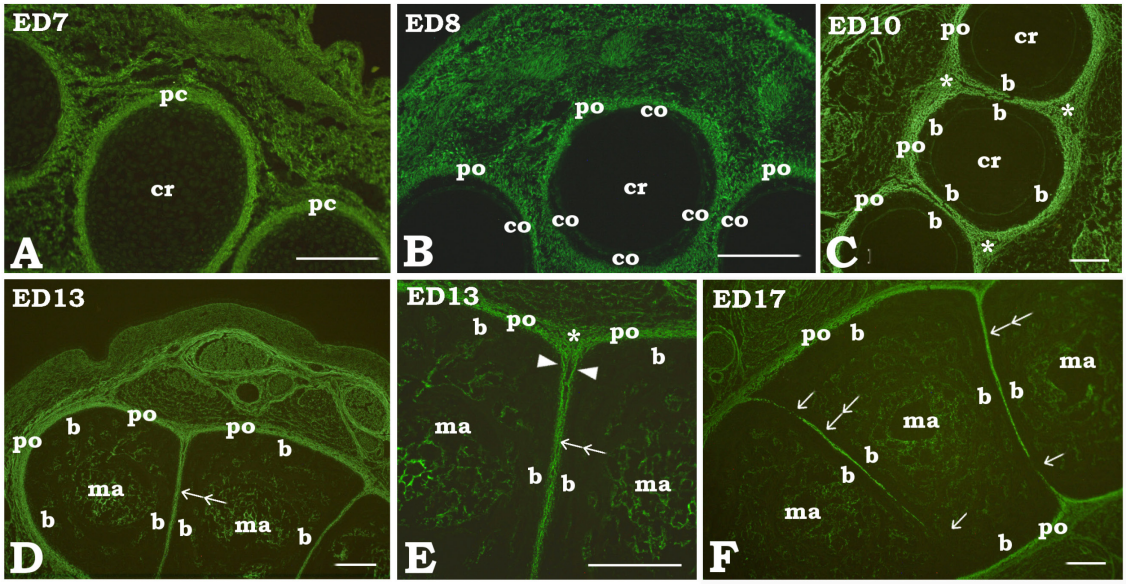

Fig. 6. Immunolocalization of fibrillin in the transversely sectioned mid-diaphysis of the TMT segment at ED7, 8, 10, 13, and 17. Intense immunoreactivities are demonstrated in perichondrium (pc) and periosteum (po) which surround cartilage rod (cr), bone collar (co) or bone cylinder (b). Arrowheads indicate periosteum coming close to each other in a back-to-back orientation, and double arrows indicate a merged periosteum between bone cylinders about to fuse. Single arrows indicate the disappearance of immunoreactivity at the site of fusion. Immunopositive matrix indicated with asterisks seems to be involved in forming a “common” periosteum which ensheathes three bone cylinders altogether. ma; bone marrow. Bars = 100 μm.

Discussion

Embryonic development of the TMT skeleton examined in this study was comprised of i) establishment of a columnar TMT segment by juxtaposing three metatarsal cartilage rods in the autopodium, ii) the onset and propagation of bone collar formation from the mid-diaphyseal portion of the cartilage, iii) longitudinal and radial growth of cylindrical periosteal bones, and iv) their lateral fusion to generate a single compound bone. Progression of bone collar formation in the TMT segment was basically similar to that in the more proximal leg segments for chick tibia and femur (Caplan and Pechak, 1987; Bruder and Caplan, 1989). In the TMT segment, however, the onsets of calcification and subsequent bony struts formation were at ED8 and 9, respectively; each were about 0.5-day behind when compared with the reported timing for the tibia (Scott-Savage and Hall, 1979; Caplan and Pechak, 1987). Subsequent radial growth, which increased the wall thickness and promoted a transition from simple bone collar to cylindrical periosteal bone, progressed in a concentric manner by centrifugal bone apposition as reported in tibia (Caplan and Pechak, 1987). However, once the surfaces of adjacent BCs came close to each other, growth toward the neighboring cylinder became spatially restricted, whereas radial growth toward the other directions continued. This pattern of differential growth observed later than ED10 delineated eventual surface configurations for a single TMT skeleton.

Among diverse bone tissue types (de Ricqlès et al., 1991), fibrolamellar bone is deposited characteristically in the long bone in birds (Castanet et al., 2000; de Margerie et al., 2002, 2004) and in their extinct species (Starck and Chinsamy, 2002). Microstructure of the chick embryonic TMT skeleton observed in this study could be categorized as a primary immature form of (and an early transitional form to) fibrolamellar bone typical in post-hatching days, because a simple bone collar developed into a thicker cylinder of cancellous woven bone consisting of trabeculae and intertrabecular channels. The channels, which appeared cancellous spaces in transverse sections, were not infilled significantly by bone deposition during embryonic development. The progress of lamellar deposition in the embryonic period, or the conversion from intertrabecular channels to lamellar osteonal units, need to be

examined in further studies, but a fluorescent labeling study of mallard's radius demonstrated that the progressive osteonal filling in woven network occurs even at 37 days in the posteclosion (de Margerie et al., 2002). Bone tissue type and its growth rate are closely related with each other, and different types of bone show different depositional rates (Amprino, 1947). Fibrolamellar bone is considered a major bone type with the fastest deposit rate, whereas avascular lamellar bone is the most slowly deposited type (Amprino, 1947; de Ricqlès et al., 1991). In this study, many lacunae for osteoblasts partly entrapped in bone were observed, implying active bone formation in the outer surface of TMT bone with fibrolamellar characteristics.

A quantitative study by de Margerie et al. (2002) validated a fundamental concept of Amprino's rule and further emphasized the significance of initial bone porosity; i.e., bone deposited with bigger cavities grows faster. In addition, periosteal bone with radially oriented primary osteons has significantly higher diametrical growth rates (de Margerie et al., 2004). These findings in posthatch development cannot be simply extrapolated to the embryonic TMT skeleton, and a relationship between bone porosity and deposition rates has still remained controversial (Starck and Chinsamy, 2002). However, because bone growth requires sufficient nutrient and mineral supplies from dense vascular network (de Ricqlès et al., 1991) and the porosity of bone reflects the degree of bone vascularization (de Margerie et al., 2005), it may be worth considering the relation of growth progression and three-dimensional orientation of channels in which vascular network resides. SEM observations in the present study showed that the formation of bony struts and trabeculae resulted in the layered arrays of channels in the cylindrical bone wall. Namely, progression of bone deposition along blood vessels is the way the channels are formed, and the orientation of channels slanted slightly to the long axis of TMT skeleton could be interpreted by a rapid longitudinal elongation and a coordinated, gradual increase of bone diameters. This causal interpretation is consistent with an explanation for faster growth in radial bone by the model derived from cross-sectioned histology of penguin long bone (de Margerie et al., 2004).

Lateral fusion of the initially independent three cylindrical bones proceeded cooperatively with the topological changes of periosteum. Fibrillin is a component of extracellular microfibrils present characteristically in the periosteal fibrous layer (Everts

et al., 1998; Yamazaki et al., 2007a), and this layer surrounds an inner osteogenic layer of the periosteum (Caplan and Pechak, 1987; Bruder and Caplan, 1989). The results of fibrillin immunohistochemistry in this study, therefore, represented a progressive back-to-back fusion of two fibrous layers and subsequent regression of the merged layer between adjacent BCs. This finding implies that independence of three tissue compartments, each consisting of a BC, a dense vascular network and a layer of osteogenic cells, was violated when a fibrous layer of the periosteum regressed. Its regression occurred first in the dorsal and ventral quarters of intervening tissue between BCs at around ED17, or at the timing of histological manifestation of bony trabeculae connecting adjacent cylinders in that region. Thus, fusion of BCs began relatively late in embryonic development, and TMT cylinders became inseparable by P1. In contrast, a single, common cavity for TMT bone marrow appeared to develop after eclosion. Cartilage in the inside of the BC is not replaced by endochondral bone but by bone marrow in birds (Caplan and Pechak, 1987), and marrow cavities are expected to be combined into a single cavity upon the fusion of cylindrical bones. However, examinations by CT tomograms in this study revealed that the septum persisted even at P1, although there existed several channels through the septum.

Fossil evidence shows that a TMT skeleton was progressively elongated in the evolution to birds from a common ancestor with theropod dinosaurs, and the fusion to form a single compound TMT bone appears to have occurred in ancient birds or their most immediate dinosaurian relatives (Dingus and Rowe, 1997). Phylogenetic studies (review by Sereno, 1999) and molecular analysis (Organ et al., 2008) indicate that modern birds are extant representatives of the diverse archosaurian clade, or more specifically, of theropod dinosaurs. Therefore, a defined, conserved molecular mechanism must be functioning to ensure the ontogenetic development of a single compound TMT bone in modern birds. To our current knowledge, there have been no molecular investigations devoted specifically to lateral fusion in the TMT skeleton. Signaling network in the closure of mouse cranial sutural space (Kim et al., 1998, Rice et al., 2000, Connerney et al., 2006) might be related to the molecular signaling during lateral fusion of TMT BCs.

In conclusion, this study has provided morphological and histological bases with several chronological landmarks meaningful for promoting further cellular and

molecular studies focusing on the development of TMT skeleton, in which lateral fusion of BCs proceeds in a temporospatially specific manner.

Chapter 2: Temporospatial distribution of osteogenic and osteoclastic cells in the development of tarsometatarsal skeleton in the chick embryo (*Gallus gallus*)

Shinji Usami, Yosuke Yamazaki, Maki Yuguchi, Yuichi Namba,
Hirofumi Kanazawa and Keitaro Isokawa
Journal of Oral Science, in press

Introduction

In appendicular skeleton of tetrapod vertebrates, there are three distinct segments named stylopodium, zeugopodium and autopodium (Rowe and Fallon, 1982; Isokawa et al., 1992), and the hindlimb autopodium basically consists of tarsal, metatarsal and phalangeal bones. In human, five metatarsal bones are not so much long in length in the middle of foot, and each of them articulated with tarsal bones in the proximal side and with phalanges in the distal side.

Compared to such human counterparts, the avian tarsometatarsal (TMT) skeleton is quite long in length, especially in terrestrial birds such as ratites, fast runners in birds, and even domestic fowl. TMT skeleton in birds spans from the base of toes to the intertarsal ankle joint, at which the bone articulates with a tibiotarsal bone in the original lower leg (Lucas and Stettenheim, 1972; Yamazaki et al., 2007a). This could be a kind of recruitment of a length of TMT to the original leg lengths, which would result in larger strides beneficial for locomotion or in other cases prey capture (Zeffer and Norberg, 2003).

It is a prime evolutionary example that the short multiple toes in the early ancestors of horse were evolved to a large and elongated foot with a single toe in the modern horse (MacFadden, 1988). What is however peculiar in avian TMT development is the lateral fusion of three initially independent tarsometatarsal bones (Namba et al., 2010). Besides, the fossil records indicate that the lateral fusion occurred in avian leg development appears to be recapitulating the changes occurred in the evolutionary history (Holtz, 1995; Dingus and Rowe, 1997; Namba et al., 2010); i.e., during a long evolution from Theropoda to the extant Aves, three independent TMT bones of Theropod species elongated, tightly packed together, fused laterally with each other, and eventually became a single compound TMT skeleton with long bone morphologies.

Previous study at the light and electron microscopic level (Namba et al., 2010), which focused on embryonic development of TMT skeleton in domestic fowl, revealed the morphological and histological details in i) establishment of a columnar TMT segment by juxtaposing three metatarsal cartilage rods in the autopodium, ii) the onset and propagation of bone collar formation from the mid-diaphyseal portion of the cartilage, iii) longitudinal and radial growth of cylindrical periosteal bones, and iv) their lateral fusion to generate a single compound bone. Thus, the time course of those changes has been largely established. In addition, among the observations made by scanning electron microscopy, a large number of lacunae for osteoblastic cells were demonstrated in the outer surface of TMT bone. It certainly implied active bone formation was in progress, but in that work, osteoblastic and osteoclastic activities have not been examined.

The present study was therefore undertaken to reveal the changes of temporospatial distribution of osteoblasts and osteoclasts in the developing TMT bone by enzyme histochemistry for alkaline phosphatase (ALP) and tartrate-resistant acid phosphatase (TRAP), with particular reference to the radial growth of individual cylindrical bone and their subsequent fusion in domestic fowl (*Gallus gallus*) at embryonic day 8-20.

Materials and Methods

Preparation of Specimens

Fertilized eggs of White Leghorn (*Gallus gallus*) obtained from Oohata hatchery (Shizuoka, Japan) were incubated at 39ºC in a humidified incubator (MTI-201A; EYELA, Tokyo, Japan). Embryos without any gross developmental defects were staged according to the morphological criteria by Hamburger and Hamilton (1951). TMT specimens excised from stage 34, 36, 39, 43 and 46 embryos were denoted as ED8, 10, 13, 17 and 20, respectively. ED20 is equivalent to the timing of hatching. Embryos (n = 8 in each EDs) were served for this study.

Specimens fixed in 4% paraformaldehyde in phosphate-buffered saline (PBS; pH 7.35) for 2 hr at 4ºC were served for examinations with the routine hematoxylin-eosin (HE) staining, αvβ3 integrin immunostaining, and the histochemistry for ALP or acid

phosphatase (ACP). All the procedures were carried out in accordance with a guideline by the Animal Experimentation Committee of Nihon University School of Dentistry, which is in compliance with the Nation Act on Welfare and Management of Animals.

Preparation of Undecalcified Bone Sections

Fixed and rinsed specimens of TMT at ED10, 13, 17 and 20 were embedded in 5% carboxymethyl cellulose (CMC), according to the procedure by Kawamoto and Shimizu (2000), and frozen in liquid nitrogen-cooled 2-methyl butane (Isokawa et al., 1994). Frozen sections at 5 μm in thickness were prepared without decalcification by utilizing adhesive Cryofilm type 1 (Sakura Finetek Co., Tokyo, Japan) according to the transfer film method (Kawamoto, 2003). Fixed and rinsed specimens at ED8, in which calcification was minimal, were frozen in an ordinary procedure for cryosections: briefly, specimens were cryoprotected in a graded series (10, 15 and 20%) of sucrose in PBS, embedded in OCT Compound (Tissue-Tek; Sakura Finetek Co.) and frozen in liquid nitrogen-cooled 2-methyl butane.

Transverse sections of TMT skeleton were prepared at the mid-diaphysis (in most cases) and at the proximal metaphysis (in some cases). Longitudinal sections along TMT skeleton were also prepared, but the findings were almost comparable with those observed in transverse sections and therefore only one case in ED8 was shown in this report.

ALP and Tartrate-resistant ACP (TRAP) Staining

Undecalcified cryosections were enzymatically stained for ALP or TRAP by utilizing reagents in TRACP&ALP stain kit (MK300; Takara Bio Inc., Kusatsu, Shiga, Japan). Briefly, the sections for examining ALP activity were equilibrated in 100 mM Tris-HCl buffer (pH 9.5) for 10 min, incubated in a substrate solution containing BCIP/NBT (for blue purple), and the reaction (or color development) was terminated at an appropriate timing by adding 20 mM EDTA to the substrate solution. The sections for examining ACP activity were incubated in a substrate solution (pH 5.0) containing NABP/FRVLB (for red purple). In examining TRAP activity, 0.5M sodium tartrate (pH 5.0) was added to the latter substrate solution immediately prior to use. Sections for observation at higher magnification were counter stained with hematoxylin. Color-

developed sections with or without hematoxylin staining were mounted in 30% glycerol and photographed with a Nikon microscope (Eclipse E600) equipped with a CCD camera (Pro 600ES; Pixera).

Immunohistochemistry

Undecalcified bone sections prestained for TRAP were equilibrated and blocked in 1% bovine serum albumin (BSA)-PBS for 1 hr, reacted with 1 to 100 dilution of mouse anti-αvβ3-integrin monoclonal antibody (Chemicon International, Inc., Temecula, CA, USA) termed MAB1976 (Cheresh and Spiro, 1987) for 1 hr and washed in PBS. Sections were subsequently incubated in fluorescein-isothiocyanate-conjugated goat anti-mouse IgG for 1 hr. After washing in PBS, sections were mounted with antifade mountant (Prolong Gold; Thermo Fisher Scientific, Waltham, MA, USA) and examined. Bright-field images for TRAP, fluorescence images for αvβ3 and their superimposed images were recorded digitally with an epifluorescence microscope equipped with a CCD camera. Controls by omitting MAB1976 or replacing it with nonimmune mouse IgG gave no specific immunofluorescence.

Results

Temporospatial Distribution of Cells Positive to ALP

The changes of distribution of ALP (+) cells were shown in an overview (Fig. 7) and in closer views (Fig. 8). Cells positive to ALP could be observed initially on the surface of mid-diaphyseal portion of rod-shaped cartilaginous TMT primordia earlier than ED8, but their distribution was soon spread towards both proximal and distal metaphyses on the surface of cartilage rods at ED8. Each of cartilaginous primordia was therefore surrounded completely with ALP (+) cells in a cross-sectioned image at the mid-diaphyseal level (Fig. 7A). In a closer view, ALP-positive blue purple ring in cross-sections appeared to contain a thin layer of bone with an indication of outward bony strut formation (Fig. 8A); a bony strut is a tiny pillar connecting two separate bone layers.

During ED10 to 20, growth of three periosteal bone cylinders (BCs), or referred as bone collar, proceeded rather quickly, and ALP (+) cells were localized mostly in the

periphery of radially growing BCs (Fig. 7B-E). At ED10, BCs were separated with each other and their cross-sectioned images were still roundish (Fig. 7B). By their further radial growth, BCs came close together, and the lateral two cylinders became a half-round shape and the remaining central cylinder changed its shape to a squared log by ED13. However, those three still remained separated at this day of development (Fig. 7C). At ED17 (Fig. 7D), BCs appeared no more separated. Trabecular structure in the diaphyseal portion of TMT was shared in considerable extent between neighboring cylinders at ED20 (Fig. 7E).

In a closer view at ED10 (Fig. 8B), it was apparent that individual BCs became double-layered, each consisting of an initial (inner) and a secondary (outer) layer, which were connected with each other by bony struts. ALP (+) cells were observed in the outer and inner surfaces of the secondary cylinder, but where the latter cylinder was not yet formed completely, cells in an outer surface of the initial cylinder were positive. Thus, the outermost part of BCs was always positive to ALP, while no ALP (+) cells were found in the tissue intervening between neighboring cylinders at ED10. Chondrocytes in the cartilage surrounded by BCs were also positive to ALP at variable levels.

At ED13 and later, double-layered cylinders characteristic at ED10 became less discernible, and the outward radial growth generated a highly trabeculated pattern in the thickened wall of TMT bone (Fig. 8C-E). Cells positive to ALP persisted in the outer two to three layers of bone trabeculae but lacked in the other large volume of TMT wall. A subset of cells positive to ALP were, however, left behind in the trabeculated TMT at ED17 and 20. These ALP (+) cells were likely to be those originally located in the outermost of BCs (Fig. 8C) and then entrapped at the plane of fusion (Fig. 8D and E). Indeed, the positive-blue purple staining in the cells left behind was diminished substantially by ED20, indicating a decrease of their ALP activities; i.e., their transition into bone lining cells, which are osteoblasts in the state of a resting or quiescent mode.

Meanwhile, erosion of cartilage occurred in BCs at ED10 and later. Eroded portion was replaced by bone marrow which was introduced to the developing TMT through blood supply. A few ALP (+) cells were observed in bone marrow as well as at the eroding surface of cartilage inside of BCs (Fig. 8C-E).

Temporospatial Distribution of TRAP-positive Osteoclasts

Although positive staining for TRAP is known to represents the presence of osteoclasts, two comparisons were made before applying TRAP staining to multiple sets of serial sections of TMT bone; i) TRAP vs an ordinary ACP staining, and ii) TRAP staining vs immunolocalization of transmembrane αvβ3 integrin, with which osteoclasts can bind to bone surface (Reinholt et al., 1990). Results of the staining of TRAP and ACP performed on the film-based undecalcified sections did not differ so much (Fig. 9A and B), but TRAP staining appeared more localized than ACP, while counterstaining with hematoxylin was effective as an alternate of HE-stained adjacent sections (Fig. 9C and D). Localization of receptor integrin (αvβ3 directed to osteopontin in bone matrix) were well matched with the TRAP staining (Fig. 9E-G). It was also shown that some of TRAP positive cells lacked fluorescence for αvβ3 (arrowheads in Fig. 9G), suggesting that migratory or yet anchored osteoclasts were also shown positive in TRAP staining.

An overview of osteoclast distribution in developing BCs of TMT was shown in solo TRAP staining (Fig. 10) and closer views in TRAP with counterstaining at ED10-20 (Fig. 11). At ED8, positive staining for TRAP was not detected (not shown).

At ED10, positive staining for TRAP was mostly localized within the wall (or mural space) of BCs, each consisting double layers connected with each other by bony struts; however, the outermost surface of the BC was negative for TRAP (Figs. 10A and 11A).

At ED13-20, TRAP (+) osteoclasts were exclusively found as scattered cells along bone marrow surface in BCs and never found within a highly trabeculated portion of TMT wall as well as in its outermost surface (Figs. 10B-D and 11B-D). The latter negative staining was also true in the fusion sites of cylinders; i.e., TRAP (+) osteoclasts were not found in the surface of bone facing the intervening tissue between neighboring cylinders (Fig. 11B and C). When the BCs fused laterally and the septal bone became marked, TRAP (+) osteoclasts were observed at bone marrow surfaces in both sides of the septa but lacked within mural space of the septa (Fig. 11D).

The above-mentioned findings were revealed by observations at the mid-diaphyseal level of TMT. Since BCs developed initially at the mid-diaphysis and extended towards proximal and distal metaphyses, findings at the metaphyseal level

were slightly belated compared to those at the mid-diaphysis. Figures 10E and 11E showed osteoclast distribution in cross-sectioned proximal metaphysis at ED17 at a low and higher magnification, respectively. In mid-diaphysis, cartilage was eroded and replaced by the tissue of bone marrow (Fig. 10C), but in the metaphyses, bone marrow was introduced partially and the remaining cartilage were still coexist, where TRAP (+) osteoclasts were observed at the bone and cartilage surfaces exposed to bone marrow, but there was none at the edge of bone adhering to yet uneroded cartilage (Figs. 4E and 11E).

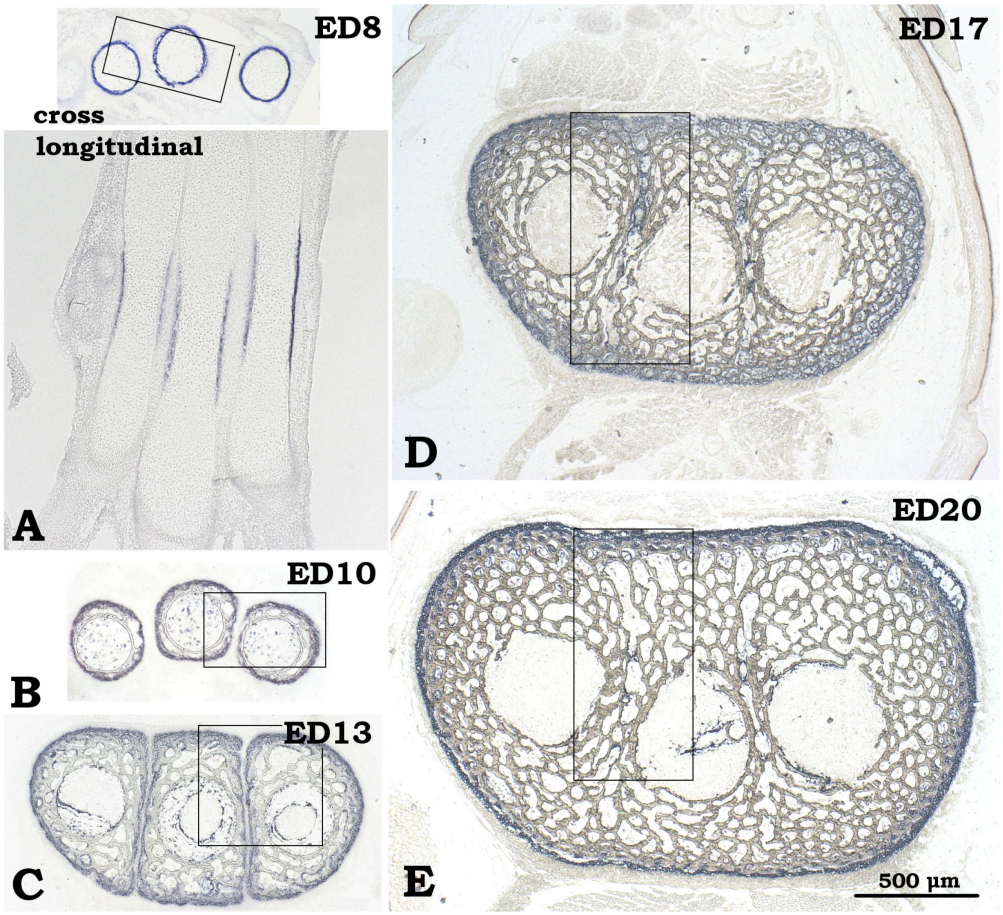

Fig. 7. Distribution of ALP-positive (in blue purple) cells in developing bone cylinders of TMT skeleton at ED8 (A), ED10 (B), ED13 (C), ED17 (D) and ED20 (E). Cross sectioned images of undecalcified TMT skeleton are shown at ED8-20, but a longitudinally sectioned image is included at ED8. Boxed areas are enlarged in Figure 8. All images are in the same magnification and a bar in E represents 500 µm.

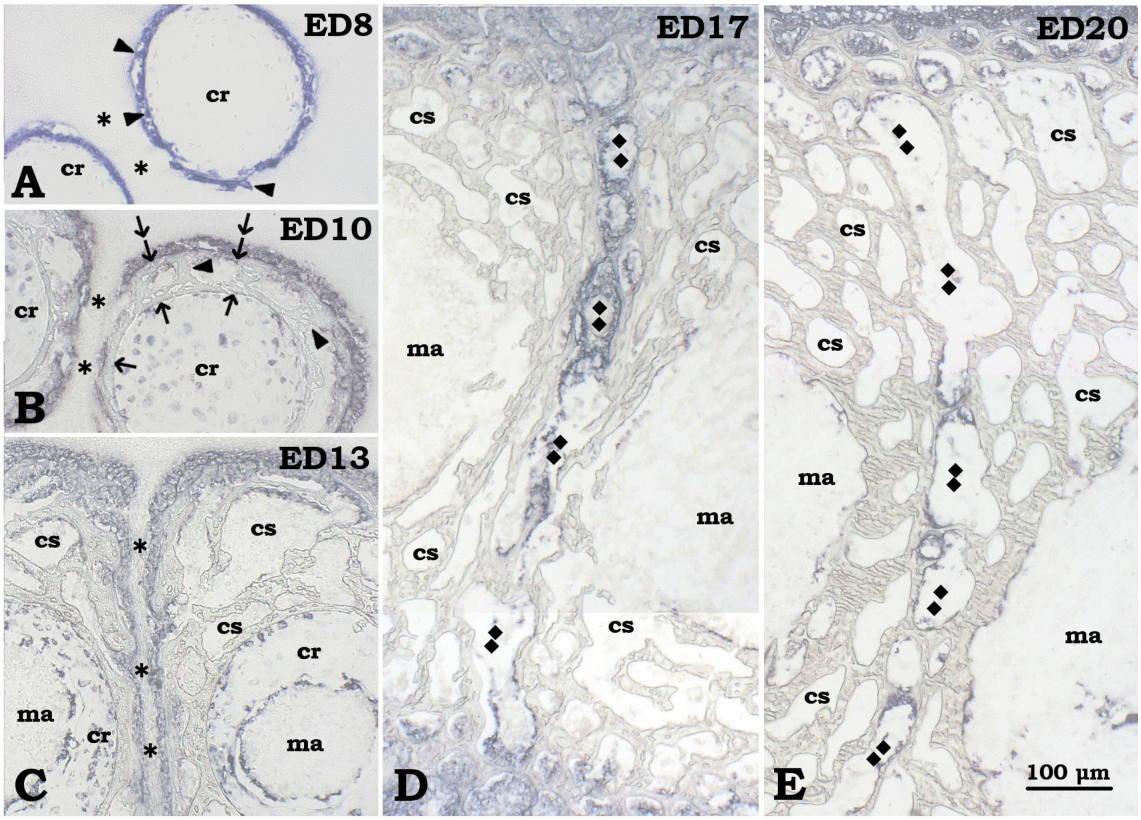

Fig. 8. Closer views in developing bone collars or cylinders stained for ALP at ED8 (A), ED10 (B), ED13 (C), ED17 (D) and ED20 (E). Boxed areas in Figure 7 are enlarged here. Bony struts in A and B are indicated with arrowheads. Inner and outer layers of the double-layered bone collars in B are indicated with single and double arrows, respectively. The intervening tissue between bone collars or cylinders in A-C is labeled with asterisks, and the plane of fusion in D and E with a row of double diamonds. Abbreviations: cr; cartilage, cs; cancellous space, ma; bone marrow. All images are in the same magnification and a bar in E represents 100 µm.

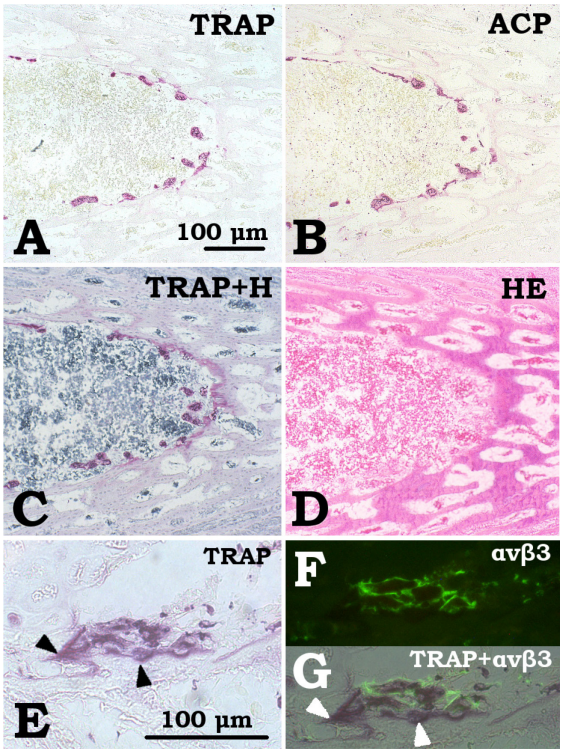

Fig. 9. Osteoclasts in the sections stained with different methods. All of the specimens are developing bone cylinders of (slight obliquely sectioned) TMT skeleton at ED17. Staining methods employed are TRAP (A), ACP (B), TRAP with hematoxylin (C), H-E staining (D) and a double staining with TRAP and anti-integrin αvβ3 (E-G); i.e., TRAP staining (E) and immunostaining (F) are superimposed in G. Each of images A-D and E-G is the same in magnification and bars in A and E represent 100 µm.

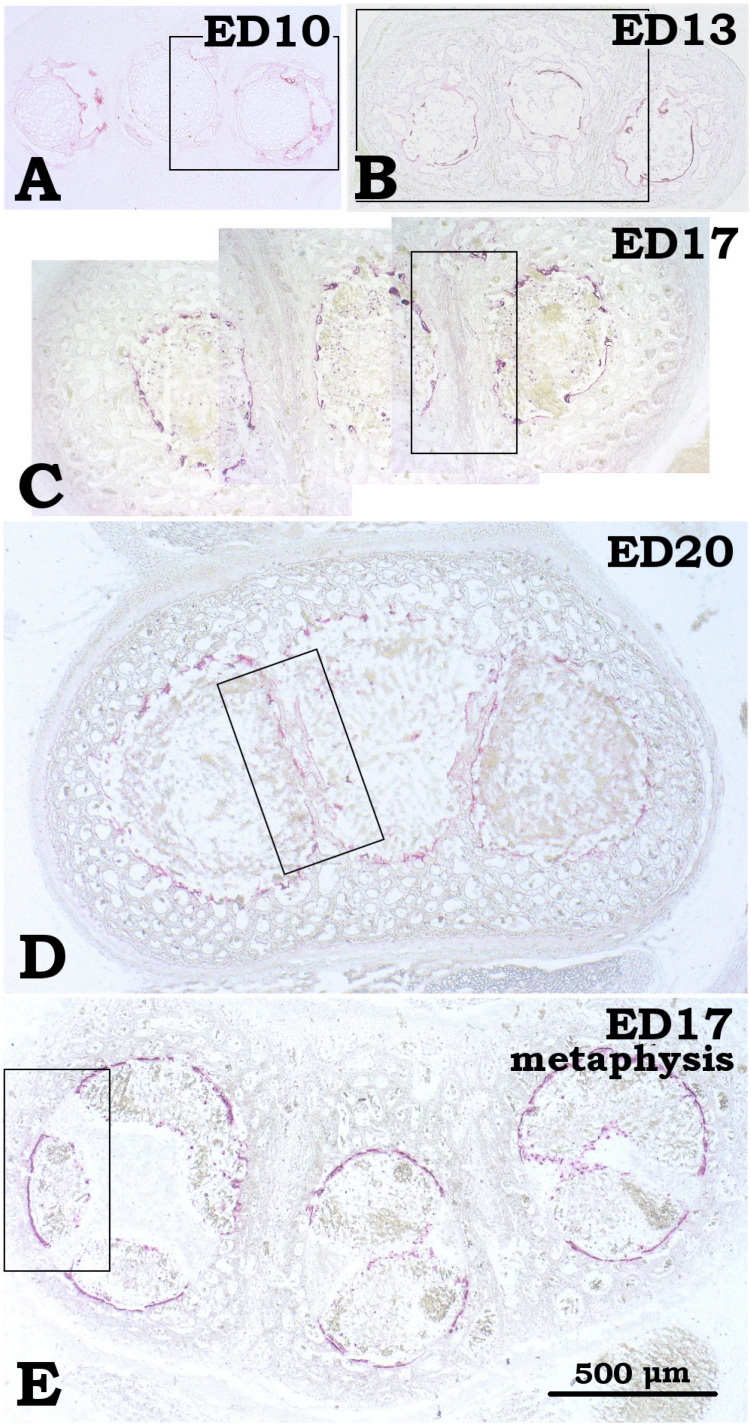

Fig. 10. Distribution of TRAP-positive (in red purple) osteoclasts in developing bone collars or cylinders of TMT skeleton at ED10 (A), ED13 (B), ED17 (C, E) and ED20 (D). Cross sectioned images at the mid-diaphysis are shown in A-D, and, for comparison, an image at the metaphysis (E) is also included. Images comparable to boxed areas in semi-adjacent sections are enlarged in Figure 11. All images are in the same magnification and a bar in E represents 500 µm.

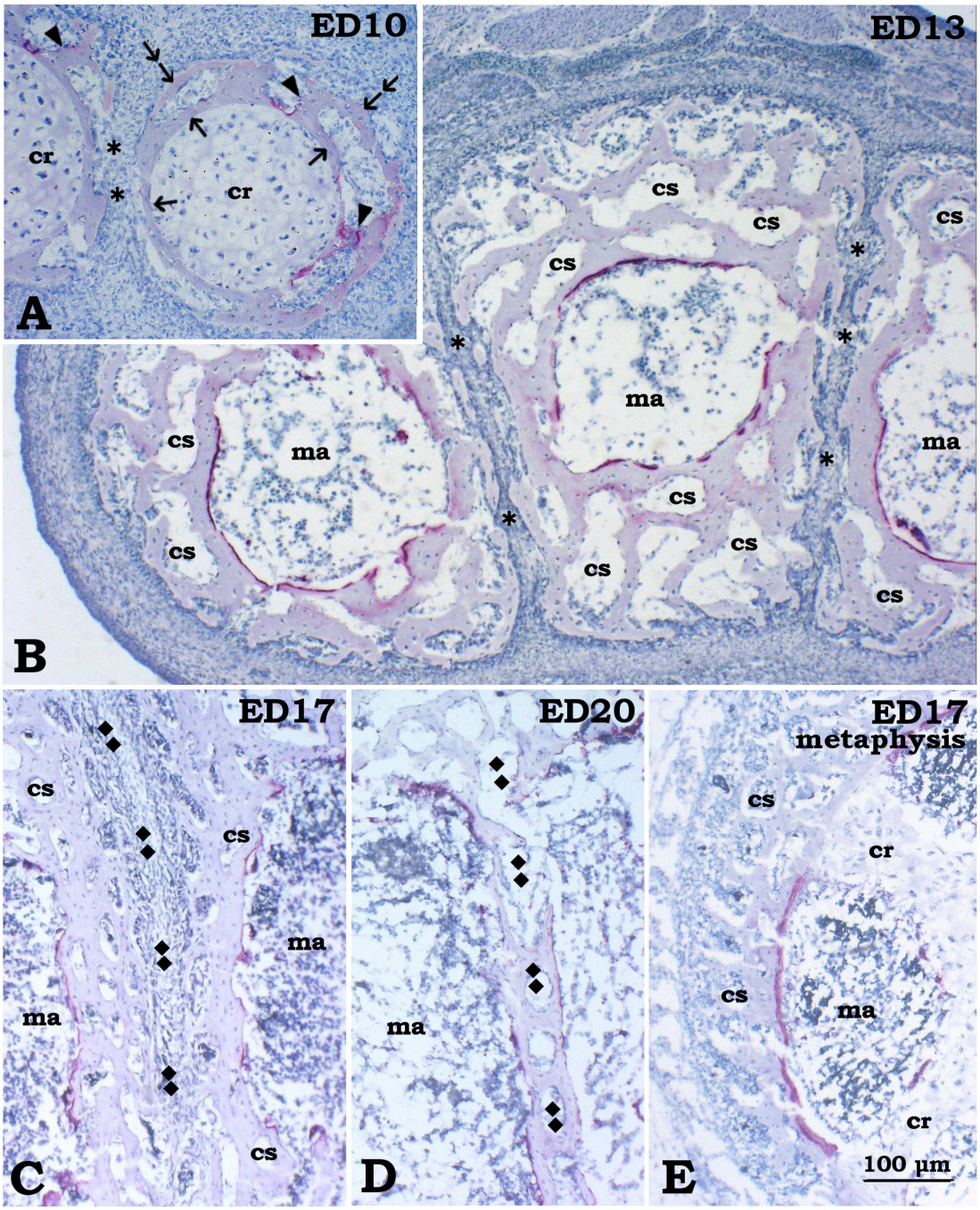

Fig. 11. Closer views in developing bone collars or cylinders stained for TRAP at ED10 (A), ED13 (B), ED17 (C, E) and ED20 (D). Images comparable to boxed areas in Figure 10 are selected in semi-adjacent sections and enlarged here. Bony struts are indicated with arrowheads, and inner and outer layers of the double-layered bone collars are indicated with single and double arrows, respectively, in A. The intervening tissue between bone collars or cylinders of TMT skeleton is labeled with asterisks in A and B. The plane of fusion in D and E labeled with a row of double diamonds. Abbreviations: cr; cartilage, cs; cancellous space, ma; bone marrow. All images are in the same magnification and a bar in E represents 100 µm.

Discussion

Enzyme histochemistry performed on undecalcified sections has demonstrated the distribution of ALP-positive cells in developing TMT skeleton. As reported in the case of embryonic chick tibial bone (Bruder and Caplan, 1989), ALP-positive cells in this study would include mature osteoblasts and preosteoblasts in the periosteal tissue but neither osteocytes nor bone lining cells (quiescent osteoblasts)(Marks and Popoff, 1988; Dobnig and Turner, 1995; Matic et al., 2016). The periosteal osteogenic cells were always localized in the periphery of a radially growing TMT bone. In previous report (Namba et al., 2010), a large number of lacunae for osteoblasts about to be imprisoned in bone matrix were demonstrated in the surface of developing bone by SEM observation. The present study has validated the SEM-finding and further shown that those cells in the periosteum are positive to ALP (Fig. 7), indicating that radial growth by active osteoblasts was indeed in progress at ED10-20. Among diverse bone types, each of which possessing different depositional rates (Amprino, 1947; de Ricqlès et al., 1991), fibrolamellar bone is characteristic in the avian long bone in both extant species (Castanet et al., 2000; de Margerie et al., 2002, 2004) and extinct species (Starck and Chinsamy, 2002). The embryonic TMT skeleton examined in previous (Namba et al., 2010) and in the present studies can be categorized as an immature form, with a rapid growth rate, of adult fibrolamellar bone.

The surface of embryonic TMT bone was not so smooth but rather trabeculated, compared to that of adult mature bone. Actually, a highly trabeculated pattern observed in cross sections at ED13 and later (Fig. 7C-E) is due to the presence of layered array of intertrabecular channels, which slanted slightly to the long axis of TMT skeleton (Namba et al., 2010). Therefore, ALP-positive osteogenic cells were demonstrated not only in the outermost surface of bone but found in a couple of layers depth of trabeculated bone.

At ED13 or later, a few cells in bone marrow or the eroding surface of cartilage inside of BCs were positive to ALP (Fig. 8C-E), which might be involved in RANKL-induced osteoclastogenesis in the milieu of endosteal side (Raggatt and Partridge, 2010). However, except for those few cells, osteoblasts left away from the peripheral zone lost

their ALP activity quickly and became flattened lining cells (quiescent osteoblasts), and thus intertrabecular channels (or cancellous spaces) were also left open widely. The latter finding would be particularly noteworthy, because it meets Amprino's rule, which has validated and interpreted by de Ricqlès et al (1991) as that the bone with larger cancellous spaces grows faster. Also reported is a fluorescent labeling study of mallard's radius demonstrated that the progressive osteonal filling in woven bone network persisted even at 37 days in the post-eclosion (de Margerie et al., 2002). These lines of evidence indicate that a higher priority is granted to rapid radial growth in embryonic period and that the bone formation halted temporarily for osteonal filling is revitalized in post-hatching period.

The changes in distribution of osteogenic cells observed in developing individual three TMT BCs were basically identical to the cases in stylopodial and zeugopodial bones such as femur, tibia and fibula (Pechak et al., 1986; Bruder and Caplan, 1989), being also accounted clearly in diagrammatic illustrations by Caplan & Pechak (1987). However, lateral fusion of three TMT BCs is a peculiar event. Using an antibody directed to periosteal molecule, fibrillin (Isokawa et al., 2004), fibrillin was localized in an outer periosteal layer but scarce or absent in an inner osteogenic cell layer (Yamazaki et al., 2007a; Namba et al., 2010). In this study, it was visualized that osteogenic cells positive to ALP activity covered two opposite outer surfaces of neighboring cylinders. The fusion was initiated and proceeded by a limited number of trabecular bridges, which resulted in containment of ALP-positive cells, followed by disappearance of their positive staining. Such changes probably do not represent a retraction of the intervening periosteal tissue, but more likely indicate that osteoblasts placed deep in trabeculated TMT bone did enter a quiescent mode.

Contrary to osteogenic cells, osteoclasts visualized by TRAP staining were observed in the innermost surface of BCs (Figs. 10 and 11). An exception was BCs at ED10. At this day of development, positive staining for TRAP was observed within the wall of those cylinders (Fig. 10A). This pattern of staining would represent that osteoclasts are deployed to the outer side of BCs exogenously via blood supply, since osteoclastic perforations are initiated at ED9 and just underway at ED10 in the diaphyseal wall of TMT BCs (in the doctoral thesis work of Namba Y; Article ID #500000515766 in NII, Japan). Osteoclasts observed later than ED10 in the endosteal

surface of BCs are recruited from bone marrow tissue, which was introduced into the marrow cavity through intraosseous blood vessels. Those osteoclasts are actively absorbing the trabeculae of endosteal margins and enlarge bone marrow spaces progressively, since the luminal diameters of BCs did increase apparently as development proceeded (Fig. 10).

The distributions of osteogenic and osteoclastic cells were separately discussed in the above but in fact appear to cooperate with each other at a macroscopic level; i.e., the radial appositional growth of TMT bone by osteoblasts is accompanied by endosteal osteoclastic resorption in a temporospatially relevant manner. This principle might be also pertinent for the progression of fusion between neighboring BCs examined in this study. Formation of trabecular bridge between BCs resulted from osteogenic activities by separate periosteum aligned in back-to-back position, and thus could be considered as just a slight variant of radial growth. In addition, the removal of bone septum at the plane of fusion could be also considered as a variant of marrow cavity enlargement, since osteoclasts involved in this process stayed in the endosteal surface and exerted their resorptive activity against septal wall.

In our previous report based on morphology and histology (Namba et al., 2010), the presence of a defined specific mechanism for the lateral fusion in TMT bone tended to be assumed. However, it was suggested in the present study that the fusion process of BCs proceeded by utilizing cellular events constituting ordinary long bone development. In recent studies (Blitz et al, 2013; Eyal et al., 2019), a modular model of long bone development and patterning has been emphasized. This model appears well fitted to the reported evolutionary diversity in elongation, fusion and unifying the marrow cavities of BCs in the avian TMT skeleton (Zeffer and Norberg, 2003; Namba et al., 2010; Hoffmeister et al., 2014). The idea of “modularly regulated morphogenesis” might provide a clue to better understand the temporospatially specific lateral fusion in BCs investigated in this study.

Conclusions

Development of avian tarsometatarsal skeleton, which is believed to recapitulate the changes occurred during evolution to birds from their common ancestor with theropod dinosaurs, was investigated histomorphologically in the embryos of domestic fowl (*Gallus gallus*). The major findings drawn were as follows:

1. Three metatarsal cartilage rods radiating distally in the autopodium became aligned parallel to each other by ED8.
2. Calcification for bone collar formation initiated at ED8 in the surface of midshaft region of cartilage, and then bone collars extended cylindrically. Coordinately, radial growth by fabricating bony struts and trabeculae resulted in further growth of bone collars, i.e., cylindrical bone with a thicker wall.
3. The bone cylinders became closely apposed with each other by ED13, and trabeculae connecting adjacent cylinders emerged at ED17. The cylinders were stably fused and took on the surface appearance of a single compound bone by ED20, while their marrow cavities remained separated by bony septa.
4. Osteogenic cells were localized preferentially in the periosteum but lacked in the other large volume of trabeculated wall of bone cylinders. Thus, cancellous spaces in the wall remained left open during embryonic periods. Osteoclasts observed later than ED10 were localized preferentially in endosteal surfaces.
5. In the fusion of three bone cylinders, trabecular bridges were formed by periosteal osteogenic cells, and osteoclasts participated in enlargement of marrow cavities and removal of bony septum between the cavities, although the removal was limited in the embryonic periods.

These findings have defined a chronology in the ontogenetic development of tarsometatarsal skeleton. Its elongation and radial appositional growth appeared well regulated by a temporospatially relevant activities of periosteal osteoblasts and endosteal osteoclasts. The fusion process of bone cylinders was likely to progress by utilizing cellular events constituting an ordinary process of the long bone development.

Acknowledgements

I am grateful to Prof. Keitaro Isokawa and Assoc. Prof. Yosuke Yamazaki for their valuable suggestions and critical reading, and to all the colleagues in Department of Anatomy for their technical assistance and continuous encouragement.

Literature Cited

Amprino R. 1947. La structure du tissue osseux envisagée comme expression de différences dans la vitesse de l'accroissement. Arch Biol 58:315-330.

Bandyopadhyay A, Kubilus JK, Crochiere ML, Linsenmayer TF, Tabin CJ. 2008. Identification of unique molecular subdomains in the perichondrium and periosteum and their role in regulating gene expression in the underlying chondrocytes. Dev Biol 321:162-174.

Blitz E, Sharir A, Akiyama H, Zelzer E. 2013. Tendon-bone attachment unit is formed modularly by a distinct pool of *Scx*- and *Sox9*-positive progenitors. Development 140:2680-2690.

Bruder SP, Caplan AI. 1989. First bone formation and the dissection of an osteogenic lineage in the embryonic chick tibia is revealed by monoclonal antibodies against osteoblasts. Bone 10:359-375.

Caplan AI, Pechak DG. 1987. The cellular and molecular embryology of bone formation. In: Peck WA, editor. Bone and Mineral Research/5. Amsterdam: Elsevier Science Publishers B.V. p 117-183.

Castanet J, Rogers KC, Cubo J, Boisard JJ. 2000. Periosteal bone growth rates in extant ratites (ostriche and emu). Implications for assessing growth in dinosaurs. C R Acad Sci III 323:543-550.

Cheresh DA, Spiro RC. 1987. Biosynthetic and functional properties of an Arg-Gly-Asp-directed receptor involved in human melanoma cell attachment to vitronectin, fibrinogen, and von Willebrand factor. J Biol Chem 262:17703-17711.

Connerney J, Andreeva V, Leshem Y, Muentener C, Mercado MA, Spicer DB. 2006. Twist1 dimer selection regulates cranial suture patterning and fusion. Dev Dyn 235:1345-1357.

de Margerie E, Cubo J, Castanet J. 2002. Bone typology and growth rate: testing and quantifying 'Amprino's rule' in the mallard (*Anas platyrhynchos*). C R Biol 325:221-230.

de Margerie E, Robin JP, Verrier D, Cubo J, Groscolas R, Castanet J. 2004. Assessing a relationship between bone microstructure and growth rate: a fluorescent labelling study in the king penguin chick (*Aptenodytes patagonicus*). J Exp Biol 207:869-879.

de Margerie E, Sanchez S, Cubo J, Castanet J. 2005. Torsional resistance as a principal component of the structural design of long bones: comparative multivariate evidence in birds. Anat Rec 282:49-66.

de Ricqlès A, Meunier FJ, Castanet J, Francillon-Vieillot H. 1991. Comparative microstructure of bone. In: Hall BK, editor. Bone vol. 3: Bone matrix and bone specific products. Florida: CRC Press, Inc. p 1-78.

Dingus L, Rowe T. 1997. The evolutionary map for dinosaurs. In The mistaken extinction: dinosaur evolution and the origin of birds. New York: WH Freeman and Company, p 169-194.

Dobnig H, Turner RT. 1995. Evidence that intermittent treatment with parathyroid hormone increases bone formation in adult rats by activation of bone lining cells. Endocrinology 136:3632-3638.

Everts V, Niehof A, Jansen D, Beertsen W. 1998. Type VI collagen is associated with microfibrils and oxytalan fibers in the extracellular matrix of periodontium, mesenterium and periosteum. J Periodontal Res 33:118-125.

Eyal S, Kult S, Rubin S, Krief S, Felsenthal N, Pineault KM, Leshkowitz D, Salame TM, Addadi Y, Wellik DM, Zelzer E. 2019. Bone morphology is regulated modularly by global and regional genetic programs. Development 146:doi 167882

Hamburger V, Hamilton HL. 1951. A series of normal stages in the development of the chick embryo. J Morphol 88:49-92.

Hartmann C, Tabin CJ. 2000. Dual roles of Wnt signaling during chondrogenesis in the chicken limb. Development 127:3141-3159.

Hoffmeister MC, Briceño JDC, Nielsen SN. 2014. The evolution of seabirds in the Humboldt current: new clues from the Pliocene of central Chile. PLoS One 9:e90043.

Holtz TR Jr. 1995. The arctometatarsalian pes, an unusual structure of the metatarsus of Cretaceous Theropoda (Dinosauria: Saurischia). J Vertebr Paleontol 14:480-519.

Isokawa K, Krug EL, Fallon JF, Markwald RR. 1992. Leg bud mesoderm retains morphogenetic potential to express limb-like characteristics (“limbness”) in collagen gel culture. Dev Dyn 193:314-324.

Isokawa K, Rezaee M, Wunsch A, Markwald RR, Krug EL. 1994. Identification of transferrin as one of multiple EDTA-extractable extracellular proteins involved in early chick heart morphogenesis. J Cell Biochem 54:207-218.

Isokawa K, Sejima H, Shimizu O, Yamazaki Y, Yamamoto K, Toda Y. 2004. Subectodermal microfibrillar bundles are organized into a distinct parallel array in the developing chick limb bud. Anat Rec 279:708-719.

Kawamoto T. 2003. Use of a new adhesive film for the preparation of multi-purpose fresh-frozen sections from hard tissues, whole-animals, insects and plants. Arch Histol Cytol 66:123-143.

Kawamoto T, Shimizu M. 2000. A method for preparing 2- to 50-µm-thick fresh-frozen sections of large samples and undecalcified hard tissues. Histochem Cell Biol 113:331-339.

Kelly WL, Bryden MM. 1983. A modified differential stain for cartilage and bone in whole mount preparations of mammalian fetuses and small vertebrates. Stain Technol 58:131-134.

Kim HJ, Rice DP, Kettunen PJ, Thesleff I. 1998. FGF-, BMP- and Shh-mediated signalling pathways in the regulation of cranial suture morphogenesis and calvarial bone development. Development 125:1241-1251.

Lucas AM, Stettenheim PR. 1972. Avian anatomy. Integument. Part I and II. Agriculture handbook 362. Washington, DC: US Government Printing Office.

MacFadden BJ. 1988. Horses, the fossil record, and evolution: a current perspective. Evol Biol 22:131-158.

Marks SC Jr, Popoff SN. 1988. Bone cell biology: the regulation of development, structure, and function in the skeleton. Am J Anat 183:1-44.

Matic I, Matthews BG, Wang X, Dyment NA, Worthley DL, Rowe DW, Grcevic D, Kalajzic I. 2016. Quiescent bone lining cells are a major source of osteoblasts during adulthood. Stem Cells 34:2930-2942.

Morse A. 1945. Formic acid-sodium citrate decalcification and butyl alcohol dehydration of teeth and bones for sectioning in paraffin. J Dent Res 24:143-153.

Namba Y, Yamazaki Y, Yuguchi M, Kameoka S, Usami S, Honda K, Isokawa K. 2010. Development of the tarsometatarsal skeleton by the lateral fusion of three cylindrical periosteal bones in the chick embryo (*Gallus gallus*). Anat Rec 293:1527-1535.

Organ CL, Schweitzer MH, Zheng W, Freimark LM, Cantley LC, Asara JM. 2008. Molecular phylogenetics of mastodon and *Tyrannosaurus rex*. Science 320:499.

Pechak DG, Kujawa MJ, Caplan AI. 1986. Morphology of bone development and bone remodeling in embryonic chick limbs. Bone 7:459-472.

Raggatt LJ, Partridge NC. 2010. Cellular and molecular mechanisms of bone remodeling. J Biol Chem 285:25103-25108.

Reinholt FP, Hultenby K, Oldbergf A, Heinegårdt D. 1990. Osteopontin-a possible anchor of osteoclasts to bone. Proc Natl Acad Sci USA 87:4473-4475.

Rice DP, Aberg T, Chan Y, Tang Z, Kettunen PJ, Pakarinen L, Maxson RE, Thesleff I. 2000. Integration of FGF and TWIST in calvarial bone and suture development. Development 127:1845-1855.

Rowe DA, Fallon JF. 1982. The proximodistal determination of skeletal parts in the developing chick leg. J Embryol Exp Morph 68:l-7.

Saunders JW, Jr. 1947. The proximo-distal sequence of origin of wing parts and the role of the ectoderm. Anat Rec 99:567.

Scott-Savage P, Hall BK. 1979. The timing of the onset of osteogenesis in the tibia of the embryonic chick. J Morphol 162:453-463.

Sereno PC. 1999. The evolution of dinosaurs. Science 284:2137-2147.

Spurr AR. 1969. A low-viscosity epoxy resin embedding medium for electron microscopy. J Ultrastruct Res 26:31-43.

Starck JM, Chinsamy A. 2002. Bone microstructure and developmental plasticity in birds and other dinosaurs. J Morphol 254:232-246.

Todt WL, Fallon JF. 1986. Development of the apical ectodermal ridge in the chick leg bud and a comparison with the wing bud. Anat Rec 215:288-304.

Yamazaki Y, Sejima H, Yuguchi M, Namba Y, Isokawa K. 2007a. Late deposition of elastin to vertical microfibrillar fibers in the presumptive dermis of the chick embryonic tarsometatarsus. Anat Rec 290:1300-1308.

Yamazaki Y, Sejima H, Yuguchi M, Shinozuka K, Isokawa K. 2007b. Cellular origin of microfibrils explored by monensin-induced perturbation of secretory activity in embryonic primary cultures. J Oral Sci 49:107-114.

Yamazaki, Y, Yuguchi M, Kubota S, Isokawa K. 2011. Whole-mount bone and cartilage staining of chick embryos with minimal decalcification. Biotech Histochem 86:351-358.

Zeffer A, Norberg UM. 2003. Leg morphology and locomotion in birds: requirements for force and speed during ankle flexion. J Exp Biol 206:1085-1097.